Lateral resistance of 'rigid' pipelines and cables on rocky seabeds

Submitted to *Canadian Geotechnical Journal* on 5/4/2018

Terry Griffiths
Corresponding author
Oceans Graduate School
The University of Western Australia,
Crawley, WA 6009,
Australia
Phone +61 404684712
Email: terry.griffiths@research.uwa.edu.au

David J. White

The University of Southampton,

Highfield, Southampton

United Kingdom

(also affiliated with the University of Western Australia)

Scott Draper

Oceans Graduate School

The University of Western Australia,

Crawley, WA 6009,

Australia

Adam Leighton

School of Civil, Environmental and Mining Engineering

The University of Western Australia,

Crawley, WA 6009,

Australia

Liang Cheng

Oceans Graduate School

The University of Western Australia,

Crawley, WA 6009,

Australia

Hongwei An

Oceans Graduate School

The University of Western Australia,

Crawley, WA 6009,

Australia

Antonino Fogliani

Dept. of Civil, Environmental and Mining Engineering

The University of Western Australia,

Crawley, WA 6009,

Australia

Videos: 1

Figures: 22

Words: 5648

Keywords: Lateral resistance; On-bottom stability; Pipeline/cable; Rocky seabed; Abrasion/failure.

ABSTRACT

Accurate assessment of lateral resistance is critical to ensure the on-bottom stability and integrity of subsea pipelines and cables in the oil/gas and marine renewable energy industries. However, on rocky seabeds recommend practices provide limited recommendations on pipe/seabed interaction, suggesting only a single value for the friction coefficient of 0.6. This paper reports on a programme of physical experiments and theoretical modelling investigating the lateral resistance of pipes on rocky seabeds. It is shown that the peak and mean effective friction can significantly exceed the interface (or Coulomb) friction coefficient when the pipe diameter (D) is similar to the median rock diameter (d_{n50}). Only when the pipe diameter becomes large compared to the rock size does the mean effective friction approach the interface friction. The effective friction coefficient was found to vary with variability in rock size and shape, as well as the length of pipe relative to median rock diameter. Each of these findings is reproduced well using the theoretical model and demonstrating that the effective lateral friction coefficient maybe higher than 0.6 for mean friction, and significantly higher for peak friction. This implies that inaccuracy may exist in current design, which may be rectified using the theoretical model.

1 INTRODUCTION

In many situations subsea pipelines and cables must be routed across rocky seabeds where soft or granular soils may have been washed away by persistently aggressive waves and currents, creating challenging conditions for stabilisation. In these situations the seabed characteristics can have a huge impact on the cost of submarine pipelines (Griffiths et al., 2010) and cable installations (Sharkey et al., 2013). For example, a high number of installed wave and tidal facilities have required cable stabilisation measures (Sharkey, 2013) such as armour casings and concrete mattresses (at the EMEC site, off the Scottish coast), rock dumping (at the Wavehub site off the Cornish coast) and horizontal directional drilling (the MCT SeaGen project in Strangford Lough, Northern Ireland).

Examples of cables installed over rocky seabeds can be found at the EMEC wave and tidal test sites in the Pentland Firth (The Crown Estate, 2015) as illustrated in Figure 1. Slightly different rocky seabed conditions are also prevalent around the proposed tidal energy sites in the Bay of Fundy that feature medium to coarse gravel and cobbles (Stark et al., 2013), including potentially mobile gravel dunes as shown in Figure 1. Rocky seabeds also occur on the Australian continental shelf along hydrocarbon pipeline and cable routes, including relatively flat limestone pavements and calcarenite caprock, as described by Sims et al. (2004) and Duncan and Gavrilov (2012).

The prevailing design methodology (The Crown Estate, 2015) used to evaluate the on-bottom stability of pipelines and cables on rocky seabed for the marine renewable energy industry is DNVGL-RP-F109 (DNV GL, 2017), which was originally written for the offshore oil and gas industry for hydrocarbon-containing pipelines. This recommended practice features three different approaches to stability design, which compare the actions on the pipe/cable, including pipe weight, hydrodynamic loading and geotechnical seabed restraint. With respect to the last of these actions – i.e. the seabed resistance between pipelines and rocky seabeds - Section 3.4.6

of the recommended practice states "*The coefficient of friction μ can normally, for a concrete coated pipe, be taken as … 0.6 on rock*" where "*Rock is here defined as crushed rocks with a 50 per cent diameter fractile larger than 50 mm*" (DNV GL, 2017). While the literal interpretation of this statement suggests it is not intended to apply to the particular condition of cables on naturally occurring rocky seabeds as shown in Figure 1, this recommended approach is used widely for pipe stability design on rocky beds. This is despite the fact that the blanket adoption of $\mu = 0.6$ cannot capture different rock types or pipe coating type – noting that cables and small diameter pipelines are rarely coated with concrete, but instead have various forms of outer layer made from other materials. The use of a single value is also at odds with conventional practice for pipelines on sand and clay, where it is widely recognised that both sediment type and pipe coating affect the friction behaviour (e.g. White et al. (2012), Hill et al. (2012), SAFEBUCK (2015), and design practice usually involves direct measurement of the relevant parameters.

From the perspective of pipeline and cable design, the use of a blanket value for the effective lateral friction coefficient can lead to inaccurate stability assessment. This leads to concerns involving the reliability and integrity of cables and pipelines, which often represent single points of failure within the overall system for both oil and gas and renewables. Furthermore it has been noted (Jee, 2016), (Boehme and Robson, 2012) that up to 80% of insurance claims from wind farm operators have been cable related, hence their integrity remains critical to the financial performance of the projects. In addition to improvements in reliability, there are also potential opportunities to reduce design and maintenance costs through improved design of cables and pipes on rocky seabed. For instance, the oil and gas industry is experiencing a phase of lower commodity prices driving significant industry innovation, whilst the offshore wind industry is experiencing a fall in subsidies while also attempting to 'close the gap' to the installed cost of non-renewable energy.

Motivated by these integrity and cost drivers, the objectives of this research are to improve understanding of the interaction between subsea pipelines and cables on rocky seabeds, particularly focusing on the resulting geotechnical lateral resistance to movement. The overarching aim is to develop an improved modelling approach to capture pipeline and cable interaction with rocky seabed, which is able to account for different rock types and pipeline/cable coating.

As discussed by Robertson et al. (2015), 'pipelines' and 'cables' cover a wide range of external hydrodynamic diameters (D), ranging from around 50 mm to over 1.2 m, and have a wide range of purposes, including: rigid steel pipelines comprised of monolithic steel; flexible pipes comprising un-bonded concentric layers of steel and polymeric materials; umbilicals comprising multiple cores of pipes, electric and fibre-optic wires and fillers encased in helically-wound armour wires and a polymeric sheath; and cables, primarily used for power and data transmission, typically comprising concentric layers of copper / fibre-optic cores, fillers, helically wound armour layer and a polymeric sheath. For simplicity, this paper refers to each of these applications as 'pipes' from hereon.

The remainder of this paper is set out as follows. In Section 2 an improved model for pipe-rock interaction is introduced, and the key characteristics which influence the interaction are explored theoretically. Section 3 then presents results from a series of laboratory experiments in which pipes of various diameter have been dragged across different rocky seabeds. Section 4 then back analyses the experiments using the improved model, so as to demonstrate the ability of the model to accurately capture the effective lateral friction coefficient. Discussion and conclusions are then given in Section 5.

2 THEORETICAL MODELLING

2.1 Lateral friction associated with a pipeline on rocky seabed

For the simplest case of a pipeline placed on a flat rocky seabed, classical theories (as described by Besson, 2013) can be used to assess the lateral friction between the pipe and rocky seabed. These theories assume that the frictional resistance results from microscopic asperities in each of the contacting surfaces, such that the gradient of the asperities leads, via geometry, to a calculated interface friction coefficient (or Coulomb friction coefficient), μ_0.

For the more general scenario of a pipeline on an irregular rocky seabed, the pipe may no longer move horizontally at a location where it is contact with the bed. Instead, the pipe may slide upwards or downwards at the macro-scale and so an effective lateral friction, μ_{eff}, can be introduced (Wilkinson et al., 1988):

$$\mu_{eff} = \frac{H}{V} = \frac{\mu_0 + \tan(\theta)}{1 - \mu_0 \tan(\theta)} \quad (1)$$

where H is the limiting horizontal resistance prior to pipe movement, V is the vertical reaction force at the point of contact (equal to the submerged weight per unit length of the pipe, if the seabed is flat in the direction parallel to the pipe and hydrodynamic loading is ignored), and θ is the angle at which the pipeline is moving relative to the horizontal. An important feature of Equation (1) is that it effectively separates the effect of the macro-scale seabed slope from the micro-scale surface interaction (defined by μ_0). Hence Equation (1) implicitly assumes that the roughness length scales associated with a rocky bed can be separated into macro and micro scales.

Since Equation (1) relates the lateral resistance to the vertical contact, it effectively replaces the interface friction as the appropriate friction coefficient to use in an on-bottom stability analysis on an irregular rocky seabed. With this in mind, three aspects of Equation (1) are useful to

recognise. Firstly, the equation implies that the effective friction is not symmetric between uphill and downhill sliding, as shown in Figure 2 for μ_0 values of 0.3 and 0.6. Hence the mean sliding resistance of a pipe that traverses over a 'flat' seabed with macro-scale asperity is greater than the friction coefficient for a flat seabed, and this has obvious implications for assessing the dynamic stability of a pipe. Secondly, the effective lateral friction coefficient becomes infinite as $\mu_0 \tan\theta \rightarrow 1$ (e.g. with a μ_0 of 0.6, a wall steeper than 59^0 causes infinite lateral resistance). Finally, the effective lateral friction coefficient becomes negative when $-\tan\theta > \mu_0$, at which point the pipe would freely slide down a slope.

2.1.1 A theoretical model for pipe on rocky seabed

With respect to developing a theoretical model to estimate the effective friction coefficient experienced by a rigid pipeline as it is dragged along on an arbitrary rocky seabed, Equation (1) can be used as the basic starting point. The only additional ingredient that is needed is to model how the pipeline conforms to the seabed so that (i) the location of the contact points can be determined and (ii) both the vertical reaction and the local angle at which the pipeline moves can also be determined at the contact points. These values can then be fed into Equation (1) to determine the effective friction coefficient for the pipe at a given location.

For convenience, in this paper it is assumed in the majority of the analysis that the pipeline is rigid and horizontal so that it has effectively only one contact point. This assumption greatly simplifies the calculation of the contact points (which is simply the highest point of contact on the seabed beneath the pipeline) and the vertical force, and needs only be adapted slightly to allow for comparison with the experiments outlined in Section 3. Nevertheless, extensions to account for pipeline flexural rigidity are reasonably straight-forward and are the subject of ongoing work by the authors.

2.2 Modelling pipelines on rocky seabeds

The theoretical model outlined in the preceding section may be used to assess the effective friction coefficient for a pipeline on any rocky seabed. In general, however, it is useful to introduce some parameters to define the pipeline and seabed, and to develop some intuition for how these parameters influence the mean and peak effective friction coefficient. With this in mind, it is assumed that the seabed is comprised of a range of rock particles having a well-defined median rock size d_{n50} (where the subscript n indicates that this refers to the rock particle size rather than the corresponding sieve mesh opening size), a coefficient of uniformity C_U and some known particle shape or angularity and a relative packing density. Dimensional reasoning and noting invariance to a transformation of dimensions then implies that:

$$\frac{\mu_{eff}}{\mu_0} = f\left(\mu_0, \frac{D}{d_{n50}}, \frac{L}{d_{n50}}, C_U, Shape, Packing\ density\right). \quad (2)$$

Where D is the pipeline diameter, L is the length of rigid pipeline that is modelled (and thus defines the length over which the contact point must occur). In the following subsections each of the parameters $D/d_{n50}, L/d_{n50}$ and C_U are explored theoretically for rocky beds comprised of both circular and square particles.

2.3 Effect of relative pipe diameter (D/d)

To investigate the effect of the relative pipeline diameter on the effective friction coefficient, the friction coefficient for a pipe sliding over a $2D$ surface profile comprising circular and square (oriented at 45°) prisms is shown as illustrated in Figure 3(a) and (b). At each location along the seabed, the pipes have been lowered down until contact with the seabed just occurs. Using a central difference scheme, the gradient of the pipe paths can then be found and, in turn, the peak friction coefficient for each D/d diameter ratio. The mean friction for each D/d diameter ratio is also found by a linear average of the effective friction over a distance of d. For

the particular case of μ_0 =0.3, the mean and peak effective friction coefficients representative of all locations of the pipe on the seabed can be calculated using Equation (1) and are given in Figure 3(c) and (d) for ratios of pipe diameter, D, to seabed 'particle' diameter, d from D/d = 0.1 to 100. This figure indicates some important points. Firstly, for sufficiently large D/d (> ~40 in Figure 3(c) and (d)), the influence of seabed particle size is substantially diminished and the sliding profiles of the pipes become 'smooth', with peak effective friction coefficient being less than 10% greater than the interface friction and mean friction coefficient being less than 0.03% greater. In contrast, for small D/d (< 40) the influence of seabed particle size becomes increasingly important in determining both the mean and peak effective friction coefficients; in the particular examples considered for the square particles there is a cut-off of peak friction which corresponds to the pipe moving upwards at the slope angle of the seabed (θ = 45°), whereas for the circular particles an infinitesimally small pipe will face a sufficiently steep wall, giving infinite peak friction. This example therefore highlights the importance of pipe diameter, relative to particle size, on the effective friction coefficient. Only when D/d is larger than some value will the interface friction provide a good estimate of the effective friction coefficient.

Secondly, it can be noted in Figure 3(c) and (d) that the peak friction for circular particles is higher than for square, reflecting the steep edge of these particles. However, the mean friction is lower. This shows that while changes in peak and mean friction occur over similar ranges of D/d, particle shape affects the relative ratio of peak to mean friction.

2.4 Effect of relative pipe length (L/d)

The contact point for a rigid pipeline can occur at any point along its length. The effect of this on the lateral friction can be understood by introducing the concept of skyline profiles. By way of analogy, the city skylines for Perth in Western Australia and New York in the United States are presented in Figure 4. The height of the buildings comprising each city are similar, but the

difference between the outline profiles is driven by the number of rows of buildings comprising the city – Perth being much smaller than New York. If a pipe of suitable diameter were dragged over each city skyline from left to right of Figure 4, the Perth skyline is much rougher while the New York skyline is comparatively 'smooth' due to the depth of buildings contributing to the outline profile.

The relevance of these observations to the lateral resistance of a rigid pipe sliding across a rocky seabed arises because the length of the pipe is a proxy for the number of skyline rows required to represent the trajectory of the pipe when pulled laterally. In essence a longer pipe would be needed to pass over the New York skyline.

To explore the effect of effective pipe length quantitatively, Figure 5 considers a pipe being dragged over a seabed comprising several rows of uniform spherical particles of diameter d, with each row having a random relative position (or phase). The random alignment of rows of particles alters the skyline profile. Increasing the number of rows comprising the skyline (i.e. increasing the pipe length) progressively smoothens the profile.

The effect of both D/d and L/d on the peak lateral resistance are shown in Figure 5 for both square and circular particles. To calculate these results the pipe has been assumed to remain horizontal (i.e. the opposite ends cannot rise and fall with the 3D topography) so the analysis effectively follows a 2D skyline, calculating the friction at any instant based on Equation (1), with the instantaneous direction of pipe motion giving the angle θ. An ensemble of 20 simulations have been undertaken in each case given that the alignment of the rows is random. The results indicate that as the length of the pipe increases the skyline contains an increasing number of rows, and so the peak friction returns to the interface sliding coefficient, μ_0, across all D/d values. This trend is observed for both the circular and square particles, although the reduction with pipe length is slower for the square particles owing to their increased angularity.

2.5 Rock with non-uniform particle size distribution

The analysis in Section 2.4 can be extended easily to consider non-uniform particles that form irregular synthetic 3D seabeds defined by a grading with median particle diameter d_{n50} and grading width $C_U = d_{85}/d_{15}$. Figure 6 provides examples for both circular and square particles, with the orientation of the square particles fixed (in this work a Rosin-Rammler distribution has been assumed to define the particle size distribution based on d_{n50} and C_U; see (Rosin and Rammler, 1933). Assuming again that the pipe is rigid and horizontal, a 3D skyline profile is formed by aligning a number of 2D profiles, with the average lateral spacing of the profiles taken as d_{n50}. As shown in Figure 7 the size of the largest particle increases as the pipe length (and thus the number of rows of particles in the skyline) gets larger. The influence of D/d_{n50}, number of rows in the skyline (i.e. L/d_{n50}) and the value of C_U has been explored numerically for a 1 m long domain and d_{n50} of 100 mm. At least 16 independent simulations have been performed for each case, using an arbitrary interface friction μ_0 of 0.3. The ratios of absolute maximum and mean friction coefficient to interface friction coefficient have been plotted in Figure 8. The results show that

- For the special case of C_U = 1, the results degenerate to the case of uniform particle sizes;
- For all of the values of C_U and any number of rows in the skyline, the mean and maximum friction coefficients tend towards the interface friction as D/d_{n50} increases;
- As C_U increases, for a given D/d_{n50} and a given number of rows in the skyline, the mean and maximum friction coefficients tend to increase;
- As the number of rows in the skyline increases, the mean and maximum friction coefficients tend to decrease

Overall, the parameters D/d_{n50}, C_U and number of rows in the skyline all influence the effective friction coefficient, with their combined effect on the trajectory of the pipe controlling the mean and peak effective friction coefficient.

3 PHYSICAL MODELLING OF LATERAL RESISTANCE

To confirm the general findings in Section 2 physical modelling of the lateral resistance between pipe and rock has been undertaken using a purpose-built test rig. The operation of the test rig is demonstrated in Video 1.

3.1 Experimental test set-up

3.1.1 Lateral resistance test rig

The lateral resistance test rig is shown in Figure 9. The key features of the test rig are:

- Two electrically-driven constant-velocity linear actuators to push or pull a model pipe laterally over a 1 m wide by 1 m long test bed;
- The actuators pivot in the vertical plane so the model test pipe may rise and fall vertically as it traverses the model seabed, also allowing the model pipe to yaw (as defined in Figure 10) so that in general two points of contact with the seabed are maintained. This aspect differs slightly to the theoretical modelling described in Section 2 above, where the pipe remained horizontal;
- The lateral force applied to the model pipe is monitored via a calibrated load cell.

The control of the linear actuators was via a single toggle-switch driving forwards and reverse movement. The load cell and displacement transducers were monitored digitally using the data-logging system described by Gaudin et al. (2009). The calibration of the load cell accounted for the mechanical leverage of the system (Figure 9).

3.1.2 Model pipes tested

The test rig was used to push and pull model pipes of 1 m length laterally a distance of 1 m across the model seabeds. The model pipes were all of hollow steel construction, with the bottom contact points of the pipes rapidly forming 'bright' steel finishes as the rocks abraded any other surface finish. The properties of the model pipes tested are given in Table 1, and shown in Figure 11. The contact weight of the pipe on the model seabed varies slightly depending on the position of the linear actuators and therefore how much actuator weight is being born by the pipe. Thus the 'near' and 'far' measured weights give the weight gradient which has been used for calculating the pipe weight at any position along its travel.

Table 1 Model pipe properties

Pipe	Diameter [mm]	Bottom Surface Roughness Ra [mm]	Weight [N/m]		Weight Gradient [N/mm]
			Near	Far	
1	42.5	4.54	121.4	101.6	-0.02058
2	61.0	2.94	144.2	121.4	
3	101.5	4.03	188.7	169.2	
4	169.0	5.93	248.8	228.6	

3.1.3 Model rocky seabeds tested

A series of four model rocky seabeds were constructed for this research. Each test seabed was formed by placing a single layer of brown and white granite cobbles and gravels onto a thick layer of tile adhesive covering a 1 m by 1 m board of 18 mm thick plywood (Figure 12). They are generally representative of different types of irregular rocky seabed relief.

Using a representative sub-sample of >30 particles of each rock type, the following measurements were made on each particle: (i) longest and shortest lengths, and a third approximately orthogonal length; (ii) the mass; and (iii) the displacement (immersed in water).

The particles were also photographed from an inclination of 45^0 while resting on a level backdrop. The Rosin-Rammler equation was subsequently fitted by a least-squares method to obtain the median particle mass M_{50} and C_U values for each rock grading. The mean and standard deviation of each of these parameters is given in Table 2 and a plot of the measured grading curves is presented in Figure 13.

Table 2 Model rock properties

Rock Sample		L1 [mm]	L2 [mm]	L3 [mm]	Mass [g]	Density [g/cm^3]	M_{50} [mm]	d_{50} [mm]	d_{n50} [mm]	C_U [-]
Blue Gravel (BG)	Mean ±SD	13.6 ±7.7	5.8 ±2.9	8.9 ±4.1	1.4 ±1.9	2.65 ±0.02	0.45	6.6	5.5	2.19
White Round (WR)	Mean ±SD	65.3 ±9.4	34.3 ±7.6	50.2 ±8.6	171 ±67	2.64 ±0.12	164.0	47.2	39.6	1.30
White Angular (WA)	Mean ±SD	74.0 ±15.4	19.7 ±2.0	42.9 ±11.2	125 ±56	2.69 ±0.07	121.0	42.3	35.6	1.38
Brown Angular (BA)	Mean ±SD	117.2 ±31.9	55.2 ±16.1	82.9 ±20.0	694 ±475	2.51 ±0.11	521.6	70.5	59.2	1.36

3.2 Lateral resistance test matrix

As described above, the models comprised 4 pipe diameters and 4 types of rock sample, giving 16 pipe/rock combinations. Each pipe/rock combination was tested for 2 "push" and 2 "pull" traverses of the board. After each of these 4 traverses, the rock test board was rotated by 90^0 and the traverses were repeated, giving a total of 16 traverses for each of the 16 combinations of rock and pipe.

3.3 Experimental results

For each test the digital data record was post-processed to convert the signal to a force/time

history using the load-cell calibration and accounting for the mechanical advantage of the system. The lateral forces were then converted to effective friction by dividing by the pipe effective weight depending on pipe lateral position. An example of the test results is presented in Figure 15 for the Brown Angular rock and the 42.5 mm diameter pipe. These results show many discrete isolated peaks in the lateral resistance, which vary significantly in both amplitude and position for each of the 16 different test sweeps. These features were observed across all of the tests, however the amplitude and frequency of peaks varied between rock types and model pipe diameters.

On a small number of occasions (less than once per test), the force applied to a rock was sufficient to break the bond with the wooden base or to fracture a rock particle as shown in Figure 16, so the peak in resistance was capped by the strength of the test bed or the rock itself rather than the true limit of the lateral pipe-seabed friction associated with the intact topography of the model seabed. These events were rare, so have a negligible effect on the mean effective friction coefficients, but highlight the high forces applied at the pipe-seabed contact points as expected from the implications of Figure 2 for large slope angles.

The horizontal resistance data was obtained at fixed displacement intervals. By sorting these effective friction data records into descending order, the distribution of instantaneous effective friction is obtained (Figure 15). These results show that very large friction coefficients ($\mu_{eff} \geq 1$) and negative friction coefficients (when the pipe was descending such that the load cells read tension during a push stage and vice versa) occur only for relatively small fractions of the total displacement ($\lesssim$5%), as would be expected based on Figure 2.

Key aspects of the test results are summarised in Figure 17. The peak friction values always significantly exceed the median friction, which is indicative of the interface friction coefficient μ_0. The peak frictions generally increase as D/d_{n50} reduces, as do the mean frictions. The rock shape is also observed to influence the results, especially for smaller pipes and for the peak

friction measured.

Each of these figures and the above general trends are consistent with the previously described theoretical predictions, show that the theoretical framework captures the mechanisms and behaviours that underpin lateral resistance behaviour of pipes on rocky seabeds.

4 BACK-ANALYSIS OF EXPERIMENTAL RESULTS

4.1 Comparison with numerical prediction from scanned surface profiles

The results in Section 3 qualitatively corroborate the trends identified in Section 2. However, in any practical situation it is useful to have a means to quantitatively predict the lateral friction coefficient experienced by a pipe on a rocky seabed. To test the ability of the theoretical model to make quantitative predictions, back-analysis of the brown angular rock sample experiments were undertaken. To properly capture the shape and particle size distribution of this rock the experimental seabed was scanned using a 3D scanner (see Figure 18); this scanner measured the seabed with an accuracy of $\pm$ 1 mm, with a resolution of one measurement per square millimetre.

Using the scanned seabed profile it is possible to make predictions using the theoretical model in Section 2.1, provided three additional aspects are considered. Firstly, a value for the interface friction μ_0 must be defined. To estimate this value the median effective friction coefficient value measured in the experiments is assumed to equal μ_0. The rationale behind this assumption is that the pipe is expected to move upwards as much as it moves downwards as it is dragged across the rocky bed; thus the median resistance should correspond to horizontal motion, at which point $\mu_{eff} \sim \mu_0$. To sense-check this assumption, comparison to published rock / steel interface frictions by Ziogos et al. (2015) has also been undertaken. The published values range from 0.5 to 0.7 for steel roughness values Ra greater than 5 μm, and from 0.1 to 0.3 for Ra values less than this. The measured test pipe bottom surface roughnesses presented in Table 1

and median friction coefficient presented in Figure 16 fall within the range of the Ziogos et al. (2015) results.

Secondly, so as to numerically account for the limiting resistance associated with rock particle breakage, a peak effective friction coefficient of 25 is assumed where numerically resistance is predicted to be infinite.

Thirdly, in the theoretical model described in Section 2 it was assumed that the pipe was rigid and horizontal, so that it had one contact point along its length. However as observed in Video 1, the physical test pipes were free to yaw as they translated laterally. This results in two contact points and can increase the lateral resistance compared to a horizontal pipe with only one contact point (Griffiths et al., 2017). To compare the numerical predictions of lateral resistance against the measured physical lateral resistances, the vertical position and yaw angle of the pipe on 2 points of rigid contact were determined using geometric arguments as the pipe was slid laterally across the model seabed. It was then possible to define the proportion of pipe weight being taken by each of the 2 contact points as follows:

$$\frac{R_1}{Ws} = \frac{L/2 - x_2}{x_1 - x_2} \tag{3}$$

and

$$\frac{R_2}{Ws} = 1 - \frac{R_1}{Ws} \tag{4}$$

where R_1 and R_2 are the reaction forces, x_1 and x_2 indicate the contact locations along the pipeline, Ws is the total weight of the pipe and L is the length of the pipe (1 m in the tests in this paper). Combing Equation (3) and (4) with Equation (1) then leads to n general expression for the total horizontal force

$$H = R_1\left(\frac{\mu_0 + \tan\theta_1}{1 - \mu_0 \tan\theta_1}\right) + R_2\left(\frac{\mu_0 + \tan\theta_2}{1 - \mu_0 \tan\theta_2}\right), \tag{5}$$

Where θ_1 and θ_2 describe the trajectories (relative to horizontal) of each point of contact on the pipe. The effective friction coefficient then follows from $\mu_{eff} = H/W_s$.

4.1.1 Numerical simulation results

Each pipe was laid down onto the scanned numerical seabed and translated laterally across the full width in each cardinal direction. Two cases of pipe boundary condition were considered - rigid horizontal pipe which is constrained to move in 2D (as per the approach taken in Section 2) and a 'yawing' pipe which can move in 3D and compares to the boundary conditions relevant to the physical tests as shown in Figure 10. The pipe/rock contact points together with the variation in pipe end elevation are presented in Figure 18. The distribution of effective friction coefficient measurements for the example cases of brown angular rock and 61 mm pipe are compared to the 3D numerically predicted results in Figure 19. The numerical results use a value of μ_0 equal to the average median friction and adopt an effective friction factor of 25 to represent 'infinite' friction events. The comparison shows good agreement across the range of test directions and across the distributions of effective lateral resistance. The results therefore confirm that the lateral resistance of a pipe can be predicted from a suitable digital representation of the seabed surface profile.

4.2 Comparison of physical test results with numerical results for horizontal pipe on an irregular finite 3D surface profile

In order to further compare the physical experimental results with the theoretical model, a series of 16 irregular 1m long quasi-3D skyline profiles were generated using both square and circular particles as illustrated in Figure 6 for each of the physical rock sample types, matching the d_{n50} and C_U values. Consequently the seabed profile does not have the same level of detail as that in Section 4.1, but all parameters are matched except the angularity/particle shape. The yawing

nature of the physical pipeline is also not captured.

The results of the physical experiments (taken from Figure 16) are compared to the numerical results in Figure 20. With reference to these results, it can be seen that very similar trends are observed in the simulations and experiments, except that the former generally predict much lower effective friction coefficients. This observation confirms the importance of properly capturing particle shape and the contact condition between the pipe and seabed. Ignoring angularity and yawing leads to under-prediction of lateral resistance.

One advantage of the numerical calculations is that they enable the efficient investigation of various features of rock/pipe interaction which are difficult to undertake with the physical test results. One example is the correlation between particle size and the occurrence of lateral resistance peaks. Scatter-plots are presented in Figure 21 for the top 20 lateral resistance peaks versus the diameter of the largest rock located within $d_{n50}/2$ downstream of the resistance peak. These plots are presented for the 2 smallest pipes on the Blue Gravel and Brown Angular rock types. Although there is scatter in the results, Figure 21 shows that the peak resistances are associated with rocks that are much larger than d_{n50}. However the peaks in effective friction coefficient relate to the difference in height of adjacent pipe positions (and particle sizes), rather than their absolute values. This point is demonstrated by looking at the particular case from Figure 21 of Brown Angular rock and 42.5 mm diameter pipe as shown in Figure 22, where it can be observed that the peak coefficient is caused not by the largest particle, but by the largest difference in size between adjacent particles.

5 CONCLUDING DISCUSSION

In this paper a theoretical model has been introduced to determine the effective lateral friction coefficient for a rigid pipe dragged across a rocky seabed. This model was used to develop

some intuition of the effect of various parameters associated with the rock and pipe on lateral resistance. Physical experiments were then undertaken, which were found to both qualitatively and quantitatively agree well with the theoretical model.

Based on the work presented in this paper the following main conclusions have been formed:

- For a pipe on a realistic rocky seabed the effective friction coefficient can significantly exceed that due to microscopic asperities (encapsulated by the interface friction coefficient μ_0) and can vary significantly from the value of 0.6 currently quoted in industry recommended practices. In particular, large variations in both the mean and peak effective friction coefficients are observed.
- The key parameters that influence the mean and peak effective friction coefficients include the interface friction coefficient μ_0, the relative pipe diameter (D/d_{n50}), pipe length (L/d_{n50}) and the particle size distribution and shape of the rocks. In all cases, however, provided D/d_{n50} is sufficiently large (for a given pipe length and both particle size distribution and shape of rock) the mean effective friction coefficient will limit to the interface friction coefficient. The peak friction coefficient test results also appear to asymptote to μ_0, but more slowly.
- A theoretical model can be used to accurately predict the mean effective friction coefficient for a pipe on a rocky seabed, provided that the interface friction coefficient is known and the seabed profile is known to sufficiently high resolution. Developing improved methods and practices for testing interface friction coefficients for pipe coatings on rock and characterising seabed rugosity will ensure these requirements are achievable in practice.

While the results of this work contribute useful insight and understanding to the behaviour of pipes on rocky seabeds, they do not yet represent a complete description of pipe interaction

480 with rocky seabeds sufficient for general use in design. Further work which is presently
481 underway extends on the work presented herein to account for hydrodynamic loading (altering
482 the direction of loading), flexible pipelines and macro-scale variations in the seabed profile (not
483 described by the characteristics of the rock).

484

485 **ACKNOWLEDGEMENTS**

486 This research forms part of the activities of the Centre of Offshore Foundation Systems (COFS),
487 supported as a node of the Australian Research Council's Centre of Excellence for Geotechnical
488 Science and Engineering (CGSE), and through the Fugro Chair in Geotechnics, the Lloyd's
489 Register Foundation Chair and Centre of Excellence in Offshore Foundations and the Shell EMI
490 Chair in Offshore Engineering. The first author acknowledges the support of the Australian
491 Government for an Australian Postgraduate Award, the University of Western Australia for his
492 Research Studentship and a University Club of Western Australia Research Travel Scholarship.
493 The second author acknowledges the support of Shell, via the Shell EMI Chair. The third author
494 acknowledges the support of the Lloyd's Register Foundation (LRF). LRF helps to protect life
495 and property by supporting engineering-related education, public engagement and the
496 application of research.
497 Thanks to Alex Duff for all his tremendous help leading the fabrication of the LRTR, as well
498 as his enthusiastic advice and practical assistance during testing. The contribution of Shixin
499 Yang through the related research undertaken in his final year project is also acknowledged
500 with thanks.

501

REFERENCES

DNV GL, 2017. On-bottom stability design of submarine pipelines.

Duncan, A.J. and Gavrilov, A., 2012. Low frequency acoustic propagation over calcarenite seabeds with thin, hard caps. Proceedings of Acoustics 2012 Fremantle.

Gaudin, C. et al., 2009. A wireless high-speed data acquisition system for geotechnical centrifuge model testing. Measurement Science and Technology, 20(9): 095709.

Griffiths, T., White, D., Draper, S., Leighton, A. and Fogliani, A., 2017. Lateral resistance of pipes on rocky seabeds – comparison of measured values with predictions from high-resolution seabed scans and synthetic models. ASME 2017 36th International Conference on Ocean, Offshore and Arctic Engineering, Trondheim, Norway, p.^pp.

Griffiths, T.J., White, D.J. and Cheng, L., 2010. Progress in investigating pipe-soil-fluid interaction: The stablepipe jip. The Twentieth International Offshore and Polar Engineering Conference, p.^pp.

Hill, A. et al., 2012. A new framework for axial pipe-soil resistance, illustrated by a range of marine clay datasets. Offshore Site Investigation and Geotechnics: Integrated Technologies-Present and Future, p.^pp.

Robertson, M. et al., 2015. The influence of pipeline bending stiffness on 3d dynamic on-bottom stability and importance for flexible flowlines, cables and umbilicals. ASME 2015 34th International Conference on Ocean, Offshore and Arctic Engineering, p.^pp. V05AT04A045-V05AT04A045.

Rosin, P. and Rammler, E., 1933. The laws governing the fineness of powdered coal. J. Inst. Fuel., 7: 29-36.

SAFEBUCK, 2015. Safe design of pipelines with lateral buckling: Safebuck iii design guideline, Atkins, Aberdeen.

Sharkey, F., 2013. Economic challenges and optimisation of ocean energy electrical systems.

Sharkey, F., Conlon, M. and Gaughan, K., 2013. Impacts on the electrical system economics from critical design factors of wave energy converters and arrays.

Sims, M., Smith, B. and Reed, T., 2004. Bayu-undan substructure foundations: Conception, design & installation aspects. Offshore Technology Conference, p.^pp.

Stark, N., Hay, A.E. and Trowse, G., 2014. Cost-effective geotechnical and sedimentological early site assessment for ocean renewable energies. 2014 Oceans-St. John's, p.^pp. 1-8.

Stark, N., Hay, A.E., Trowse, G. and Kopf, A., 2013. Geotechnical investiogation of grand passage, nova scotia, with regard to sediment mobility and the installation of tidal energy converters. Proceedings of the European Wave and Tidal Energy Conference Series, p.^pp.

The Crown Estate, 2015. Emec pfow enabling actions project: Sub-sea cable lifecycle study.

White, D., Campbell, M., Boylan, N. and Bransby, M., 2012. A new framework for axial pipe-soil interaction, illustrated by shear box tests on carbonate soils. Offshore Site Investigation and Geotechnics: Integrated Technologies-Present and Future, p.^pp.

Wilkinson, R., Palmer, A., Ellis, J., Seymour, E. and Sanderson, N., 1988. Stability of pipelines in trenches. Proceedings of the European Seminar on Offshore Oil and Gas Pipeline Technology, p.^pp.

Ziogos, A.D., Brown, M.J., Ivanovic, A. and Morgan, N., 2015. Rock-steel interface testing and considerations for gravity foundations for tidal energy generators. Frontiers in Offshore Geotechnics III. CRC Press.

Figures

(1) at EMEC (Estate, 2015)

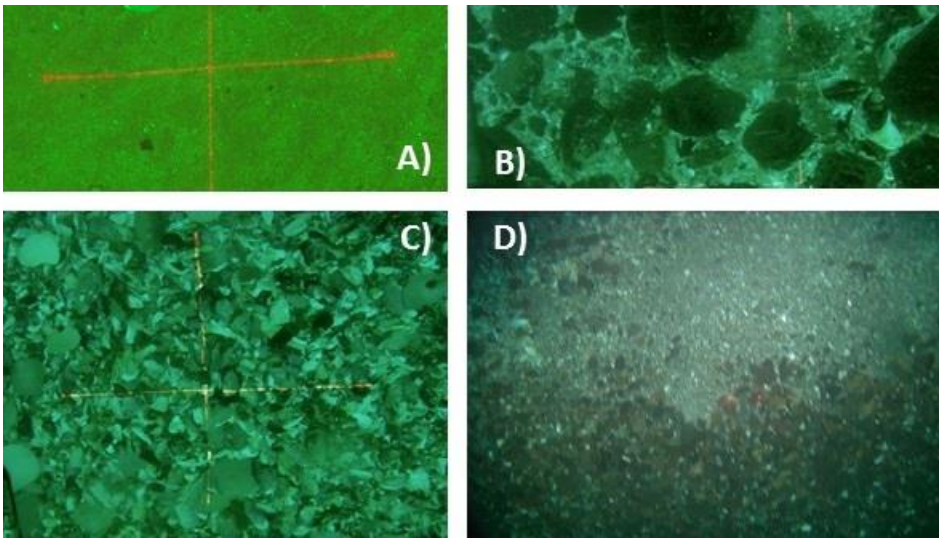

(2) Bay of Fundy (Stark et al., 2014)

Figure 1: Example rocky seabeds

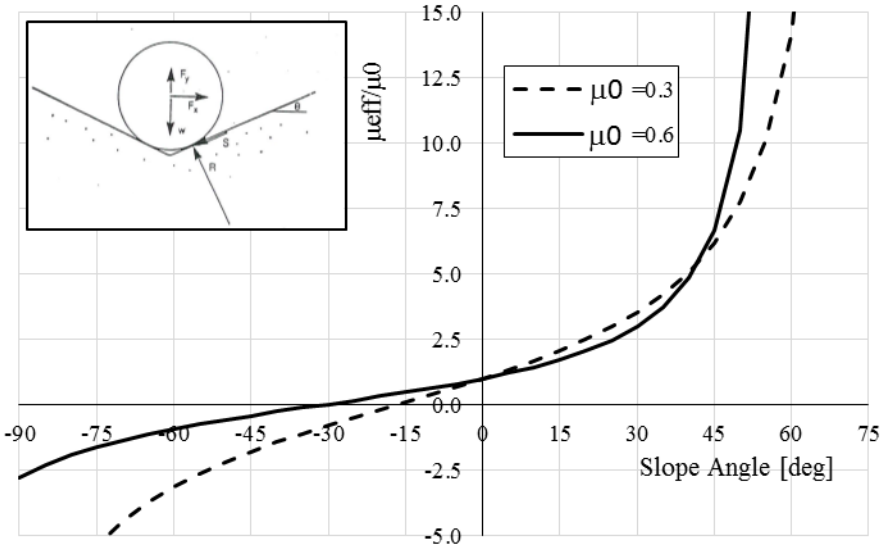

Figure 2: Pipe effective friction due to trench side-wall friction

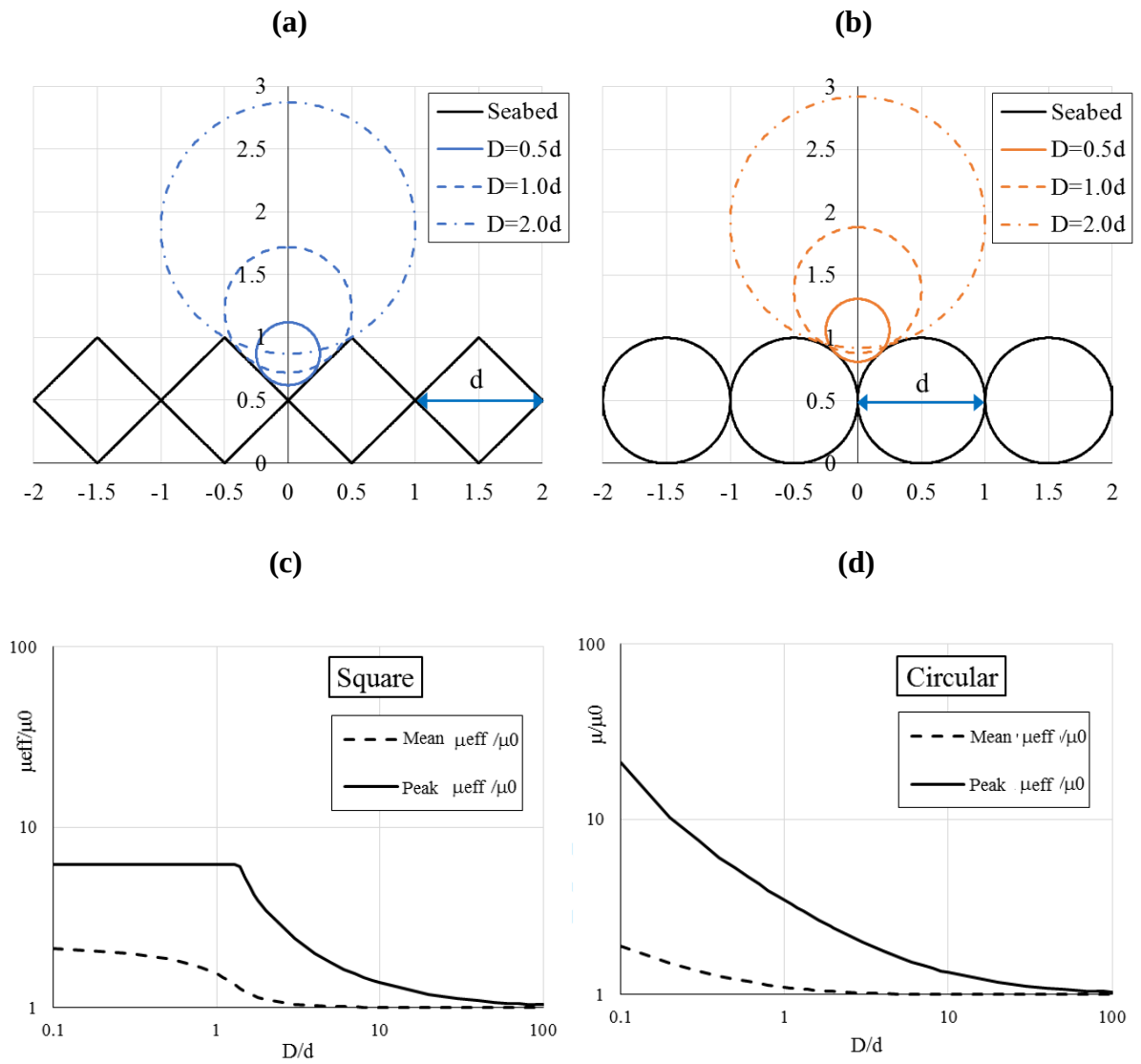

Figure 3: Pipe mean and peak lateral resistance on 2D regular seabed profiles (μ_0 = 0.3)

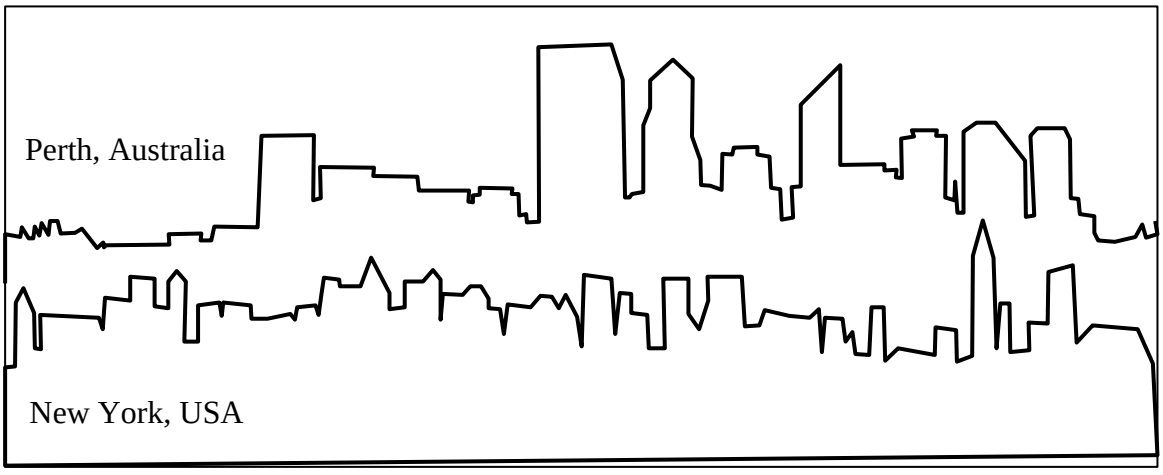

Figure 4: Example city skyline profiles

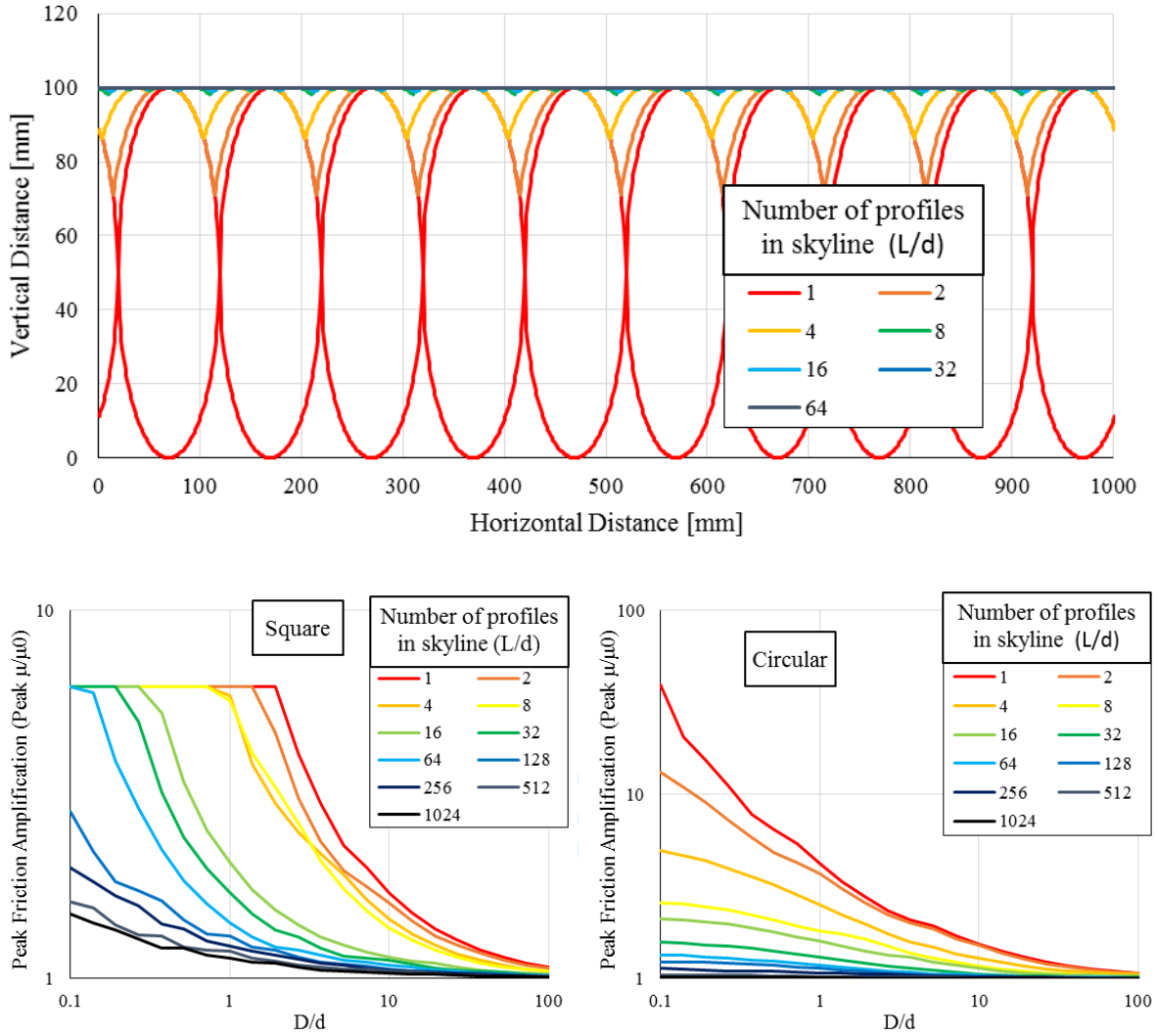

Figure 5: Variation of pipe profile gradient maxima versus D/d and number of regular square profiles in skyline

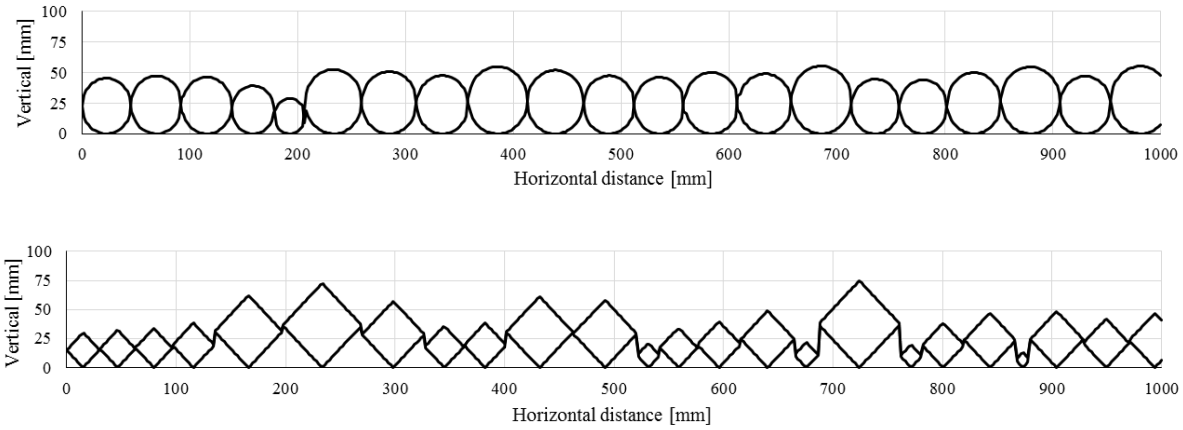

Figure 6: Irregular 2D profiles: d_{n50} = 50 mm; circular C_U= 1.3; square C_U = 2.5

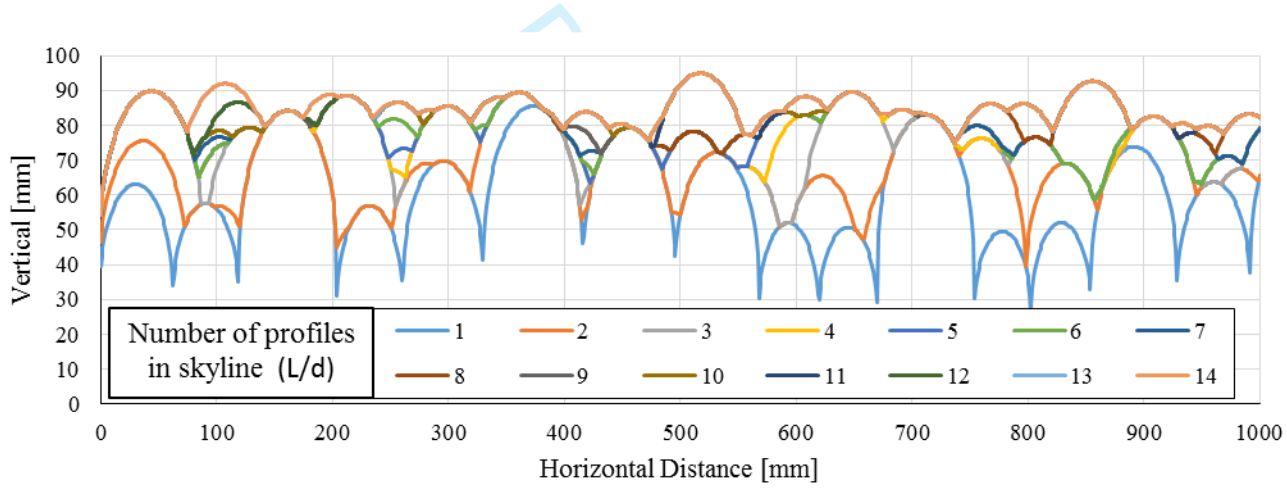

Figure 7: Cumulative skyline profile formed from irregular circular particle size distribution (d_{n50} = 59.2 mm, C_U = 1.36)

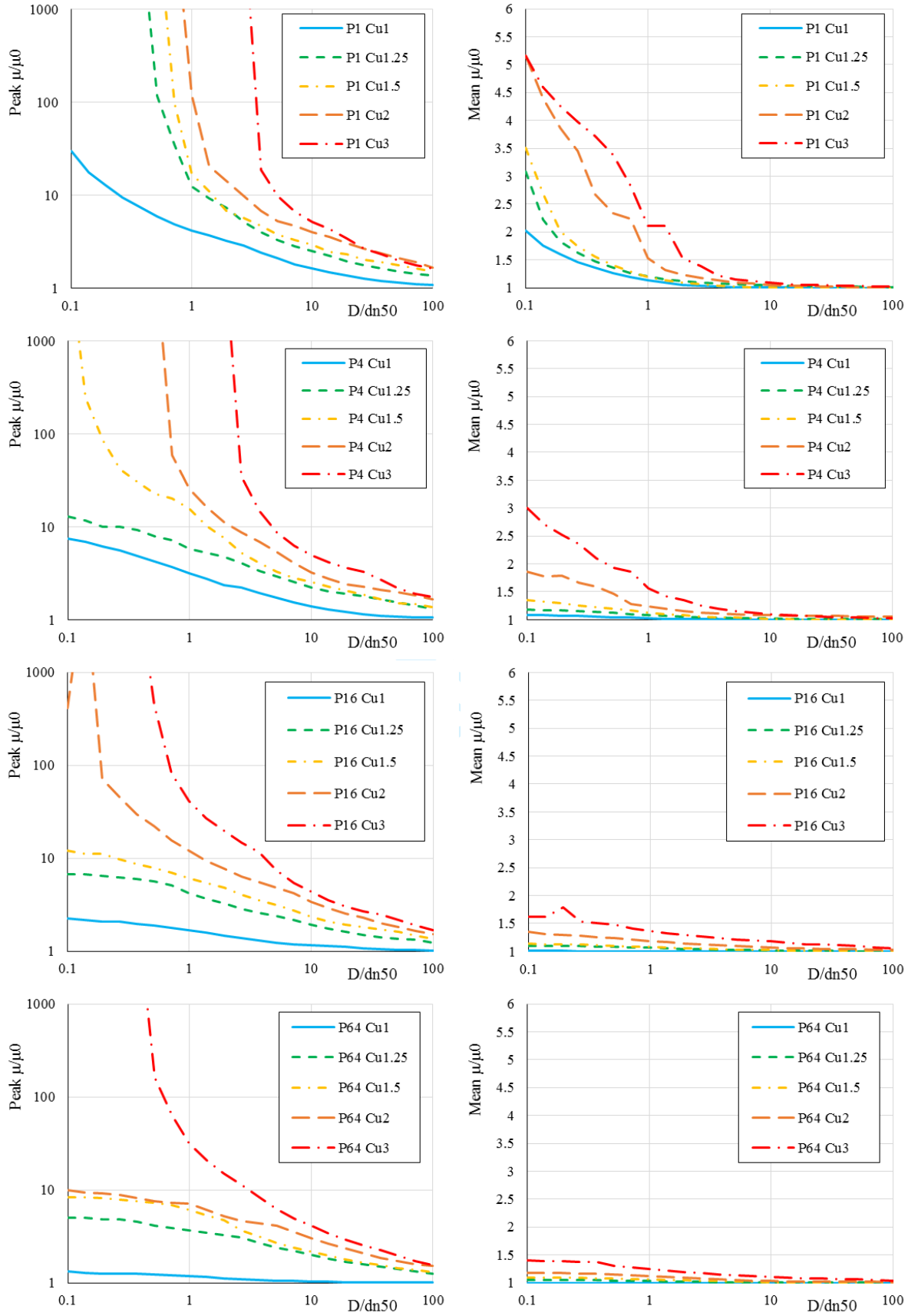

Figure 8: Comparison of pipe mean and maximum friction ratios from irregular quasi-3D circular profiles with variation in number of profiles and C_U

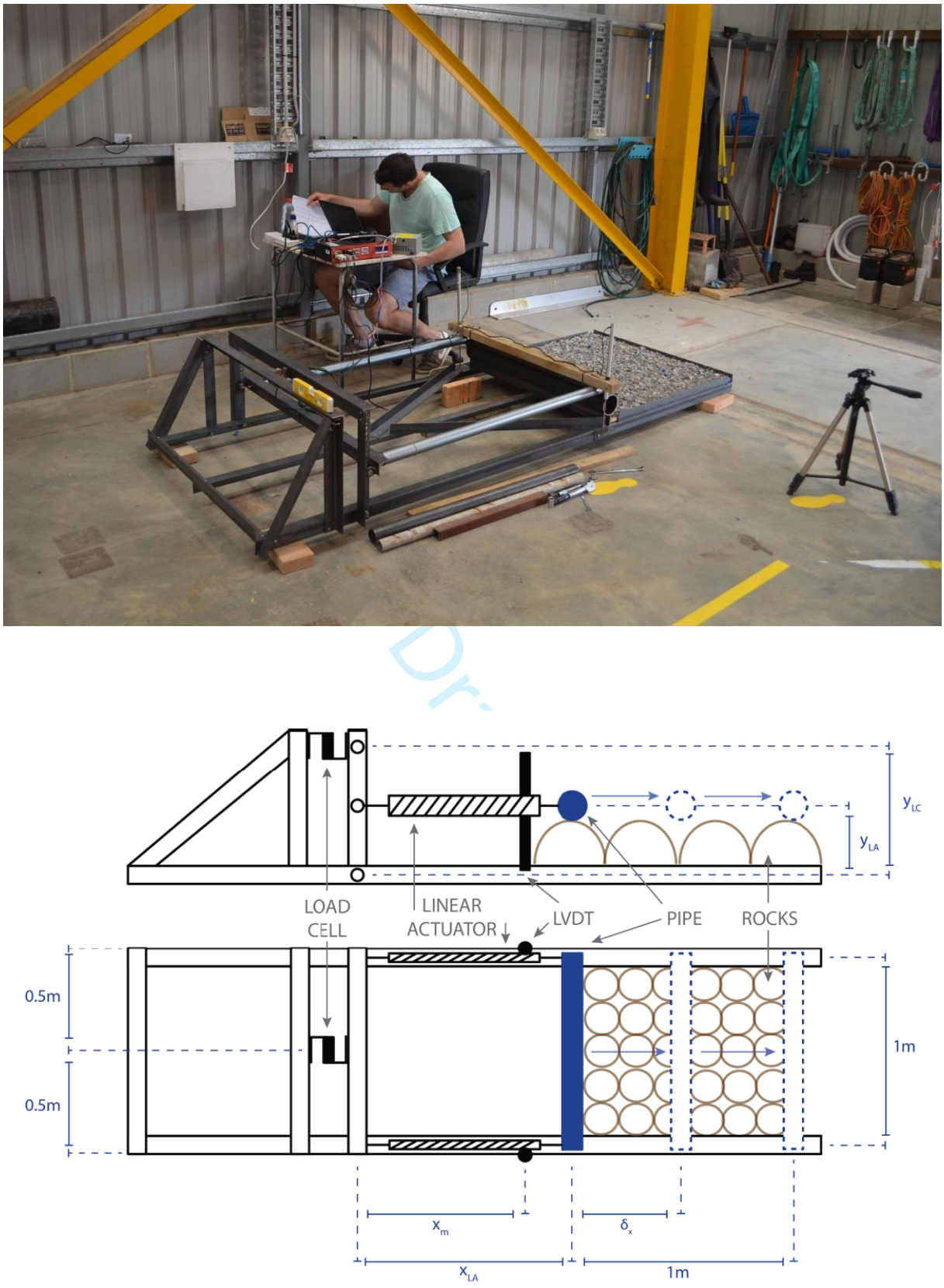

Figure 9: Photograph and schematic plan and elevation of lateral resistance test rig

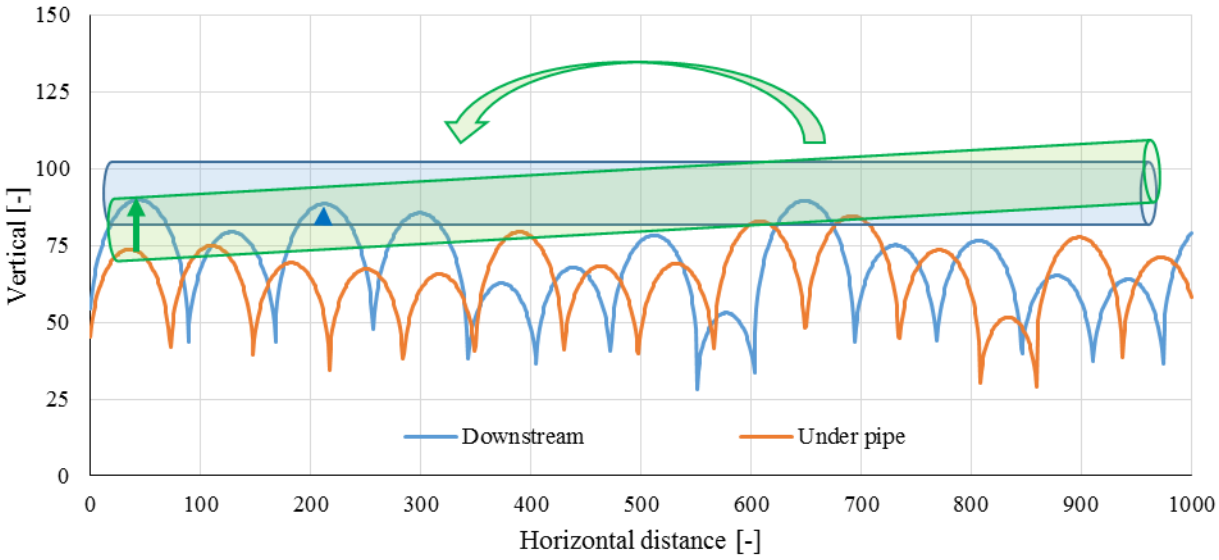

Figure 10: Effect of pipe yawing on lateral resistance over finite irregular profiles. Blue arrow shows step height for irrotational pipe compared to green arrow for pipe able to 'yaw' (d_{n50} = 59.2 mm, C_U = 1.36)

Figure 11: Four model pipes shown on round river stone test board

a) Blue Gravel stone test board b) White Round stone test board

c) White Angular stone test board d) Brown Angular stone test board

Figure 12: Stone test boards

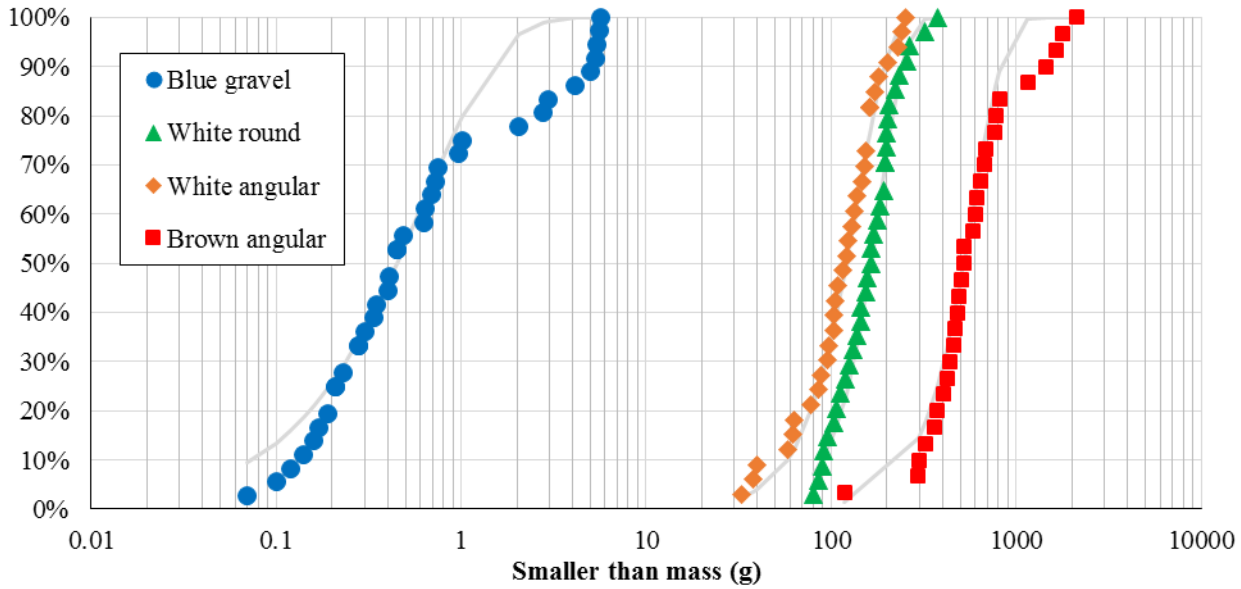

Figure 13: Rock sample grading curves (percentage passing by mass)

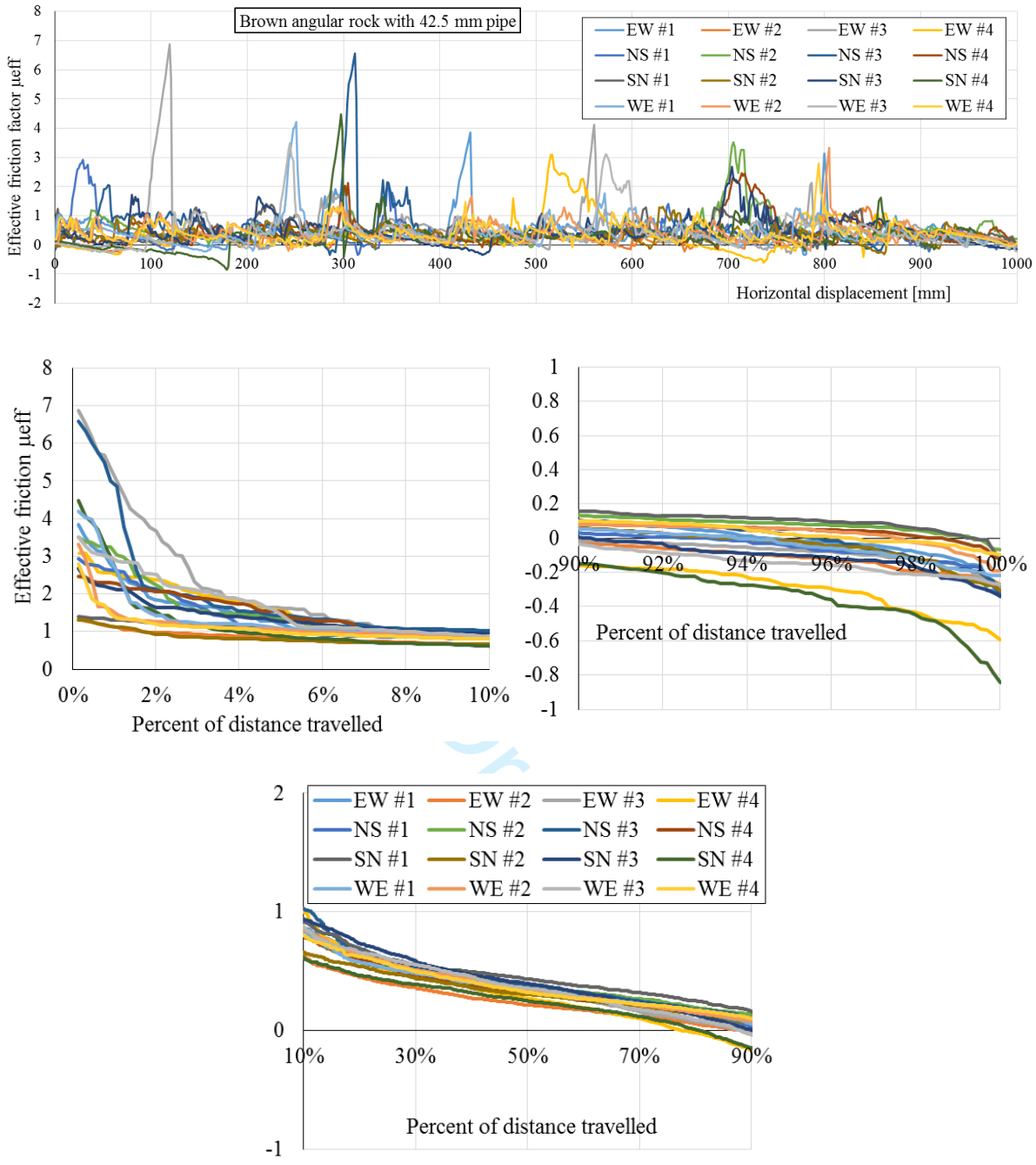

Figure 14: Effective friction factor vs displacement and sorted effective friction for Brown angular rock and 42.5 mm diameter pipe (D/d_{n50} = 0.72)

Figure 15: Testing issues – rock fracture (L) and rock/board adhesion failure (R)

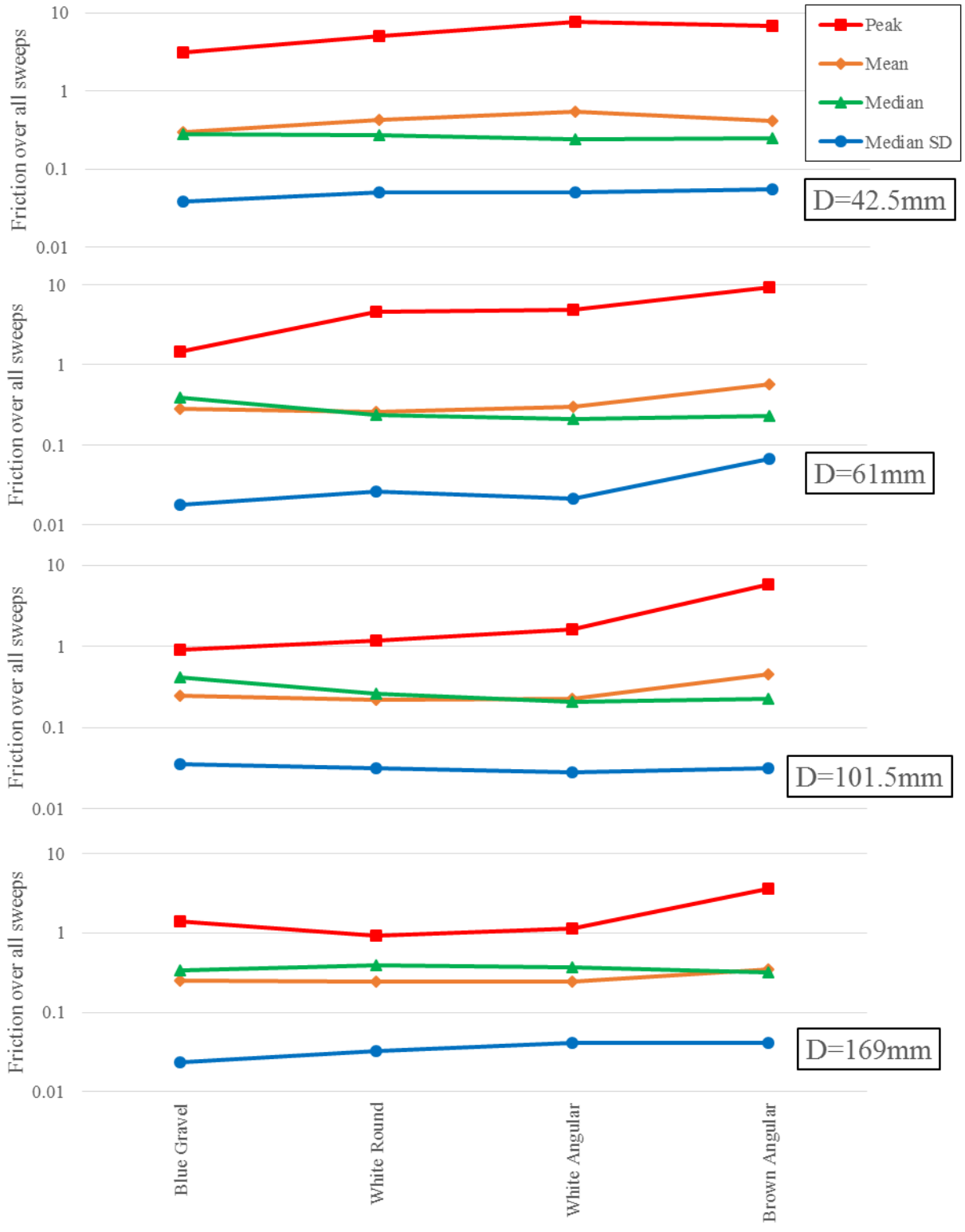

Figure 16: Physical test results summary

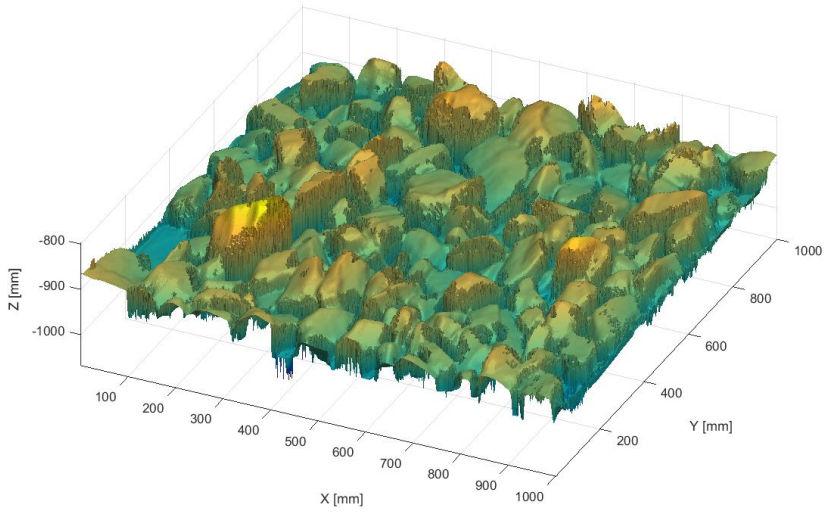

Figure 17: Scan of Brown Angular rock

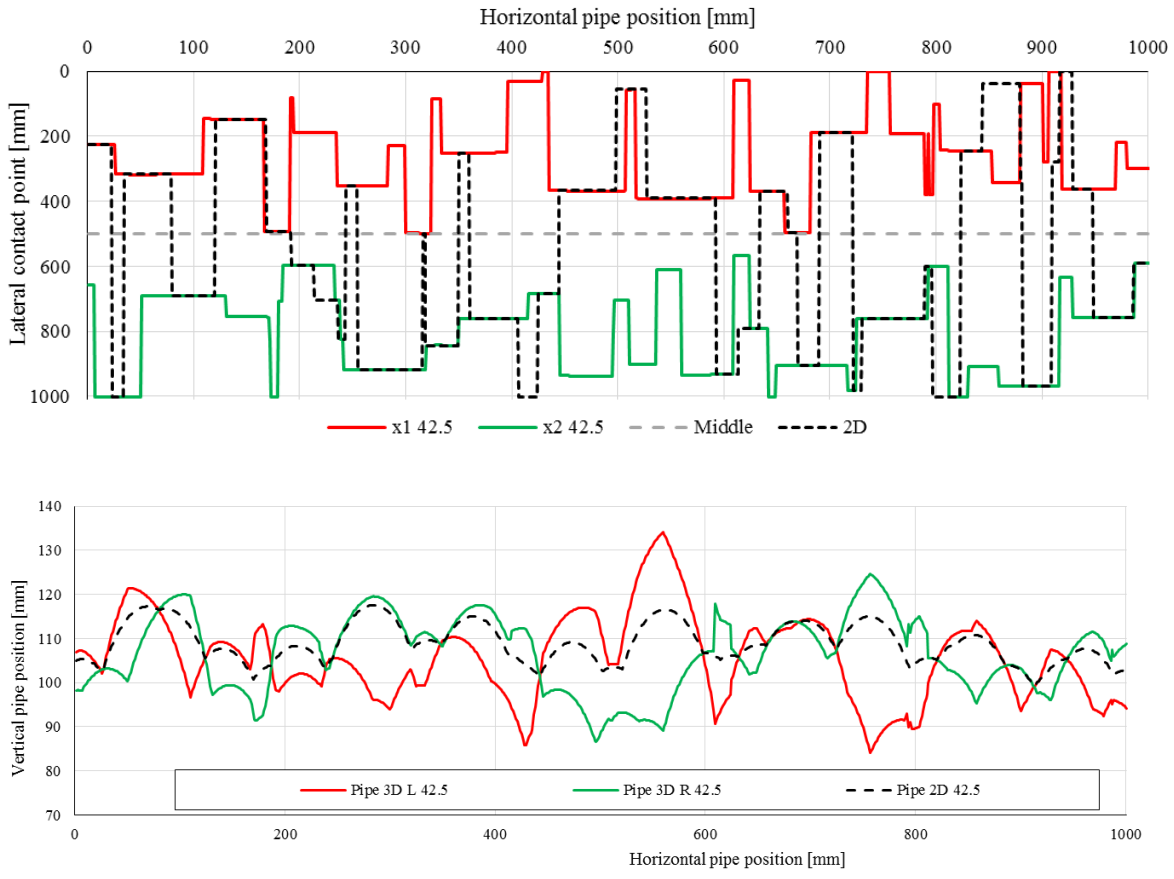

Figure 18: Lateral contact location and pipe end vertical elevation for 2D versus 3D contact as a function of lateral pipe position (Brown angular rock scan 1)

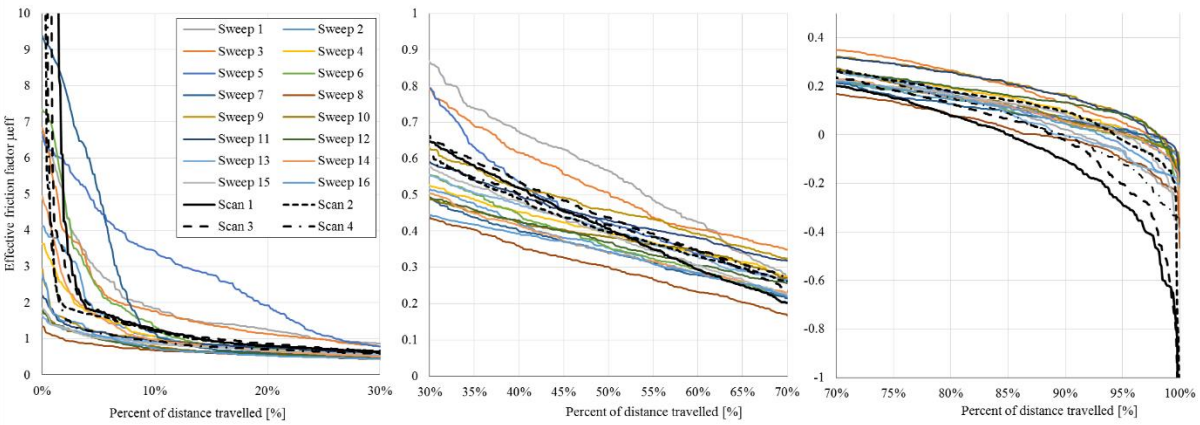

Figure 19: Comparison of effective friction distribution from scanned and measured tests (Brown angular rock, 61 mm pipe)

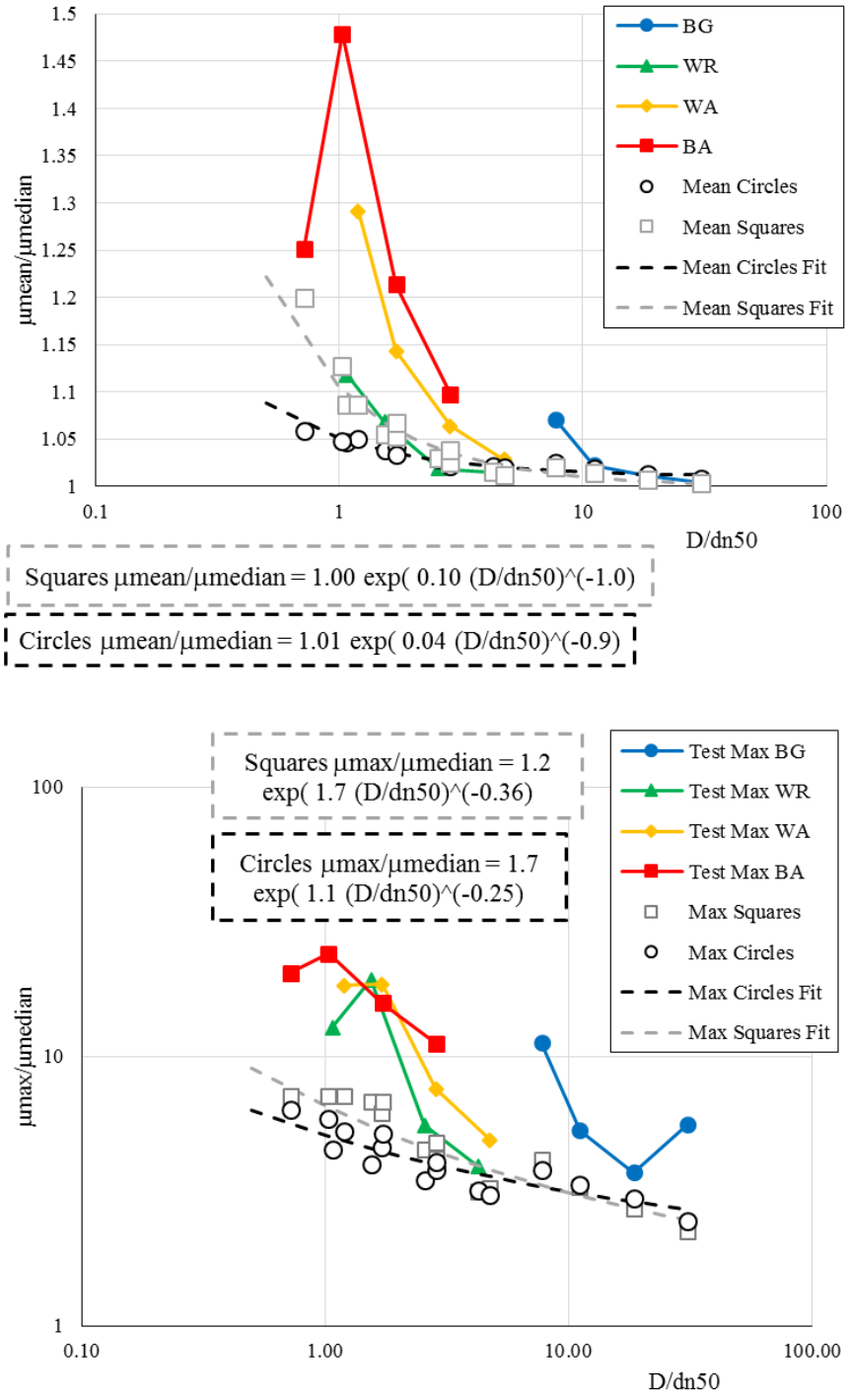

Figure 20: Comparison of maximum and mean friction amplification ratios for experimental and square / circular numerical results against D/d_{n50}

Note: it is envisaged that these plots ought NOT to be used in design practice given as-yet they only capture SOME of the necessary physics describing pipe-rock-fluid interaction

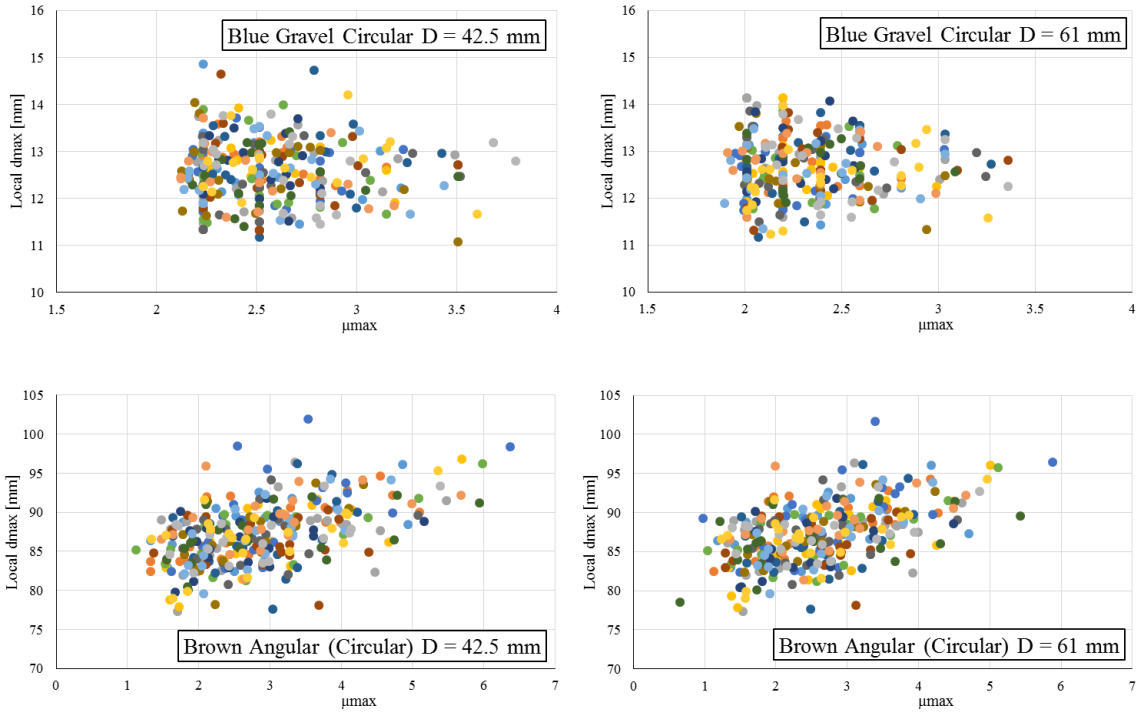

Figure 21: Comparison of synthetic simulations using spherical particles of peak friction versus adjacent maximum rock diameter

Note Blue gravel d_{n50} = 5.5 mm, d_{max} = 18.1 mm overall

Brown angular d_{n50} = 59.2 mm, d_{max} = 102.5 mm overall

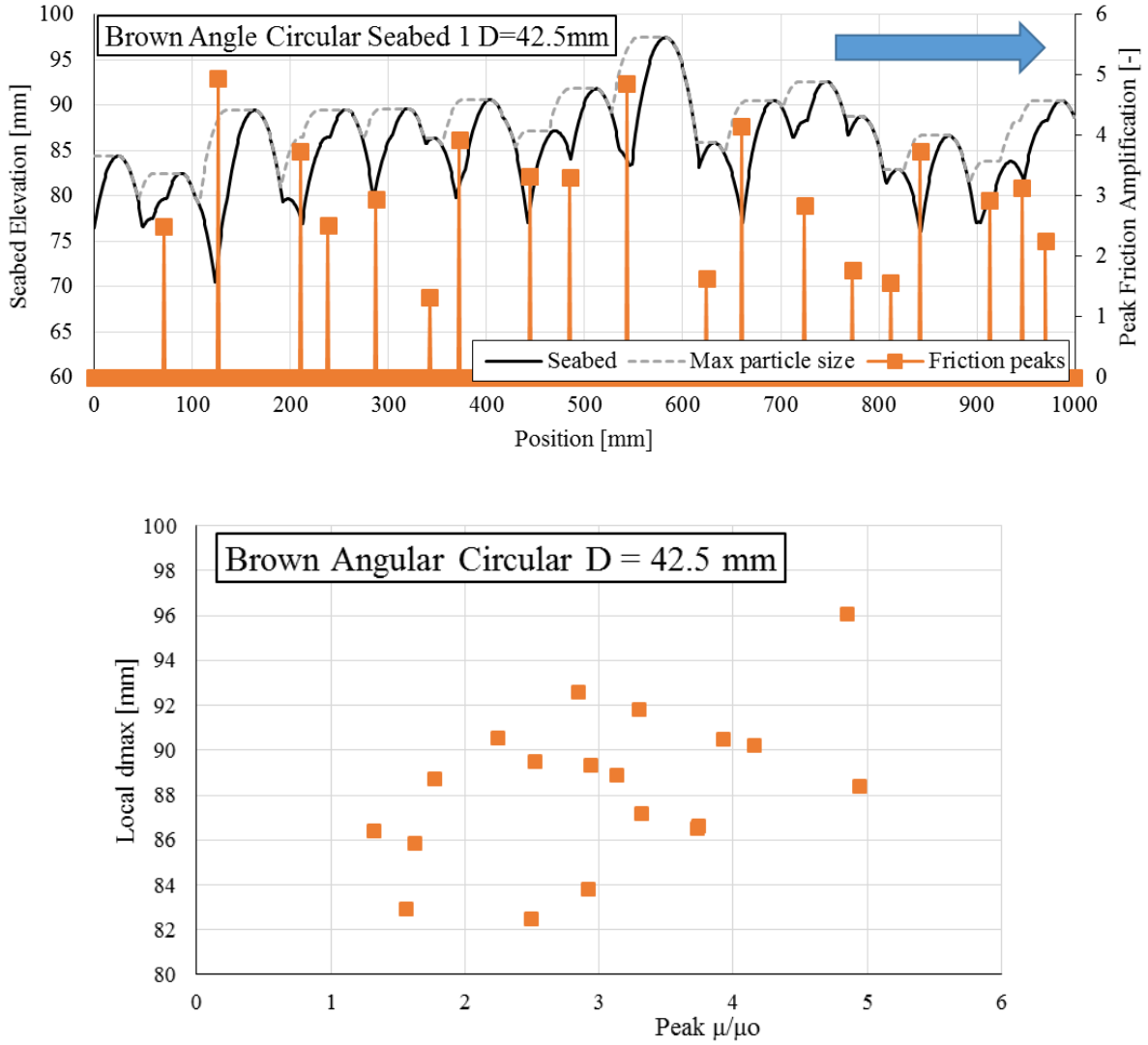

Figure 22: Correspondence between peak friction and particle size (Brown Angular rock simulation with circular particles D = 42.5 mm)